Removal of Methyl Orange Using Nanocomposites Based on Polyaniline/Nb_2O_5/MnO_2 and Polyaniline/Nb_2O_5/Cr_2O_3 as New Adsorbents

Karrar Majeed Obaid, Ahmed Saadoon Abbas, and Yahya Fahim Al-Khafaji*

Department of Chemistry, College of Science, University of Babylon, Hilla 51002, Iraq

* ***Corresponding author:***

email:
sci.yahya.alkhafaji@uobabylon.edu.iq

Received: February 19, 2023
Accepted: May 17, 2023

DOI: 10.22146/ijc.82417

Abstract: *Dyes are the most widely employed materials for coloring applications, especially for industrial purposes; thus, dyes are applied in the textile, cosmetics and foodstuffs. Dyes are very important owing to their applications in all aspects of human life. Accordingly, the production volume of dyes around the world is increasing. In this study, a new type of multifunctional material: polyaniline/Nb_2O_5/MnO_2 and polyaniline/Nb_2O_5/Cr_2O_3 nanocomposites, was prepared by chemical polymerization from aniline monomer in the presence of metal oxides (Nb_2O_5, Cr_2O_3, and MnO_2) and an oxidant (ammonium persulfate) in acidic aqueous solution for the elimination of dye from water. Herein, the nanocomposite was found to be a favorable adsorbent for wastewater treatment due to its high adsorption and efficiency, self-regeneration quality, low cost and easy synthesis. Fourier transform infrared spectroscopy, X-ray diffraction, scanning electron microscopy and UV-visible spectroscopy were used to assess the synthesized nanocomposites' characteristics. From the results, we discovered that polyaniline nanocomposites doped with Nb_2O_5 and MnO_2 nanoparticles had a higher adsorption efficiency (~97.37%) than those found in polyaniline with Cr_2O_3 and MnO_2 (~94.3%). We looked at the adsorption conditions, including the medium's pH, the initial dye concentration, the dosage of the adsorbent, and the adsorption time.*

Keywords: *adsorption; dye removal; polyaniline; metal oxide*

■ INTRODUCTION

Dyes are the most widely employed materials for coloring applications, especially for industrial purposes. Dyes are used for textiles, cosmetics, foodstuffs and anticorrosion [1]. Dyes are very important due to their application in all aspects of human life. Accordingly, their production volume around the world is increasing. Over the last few decades, more attention has been placed on the discharge of about 10–15% of the dyes into the environment. So, there is a major environmental problem arising from the frequent colored wastewater, which is eco-toxic and hazardous in nature. In addition, the quality of water is decreased due to the dyes. Examples of such dye are methyl orange (MO). With this in mind, the treatment of dyes or dyestuffs before their discharge into the environment needs more attention.

Two types of recent treatment techniques could be used: chemical and physical treatment; examples of such techniques are liquid chromatography, precipitation, ion exchange, and electrochemical [2]. However, the problems with these techniques are that they are expensive, and some of them are not effective. Subsequently, researchers are trying to find other techniques that are not expensive, more active, easy to use and able to be recycled for use multiple times to remove dye from wastewater. Researchers have been investigating several selective adsorbent materials in this area, such as zeolites, chitosan, and clay [3-4]. Owing to the fact that conducting polymer nanomaterials have various chemical and physical possessions, they have been employed in many applications as they are easy to prepare, have a low cost and allow ease of doping polymers polyaniline (PANI) as shown in Fig. 1.

PANI has two functional groups, amine and imine, that facilitate the adsorption of dyes such as MO. Adsorption mechanisms can be affected by many factors

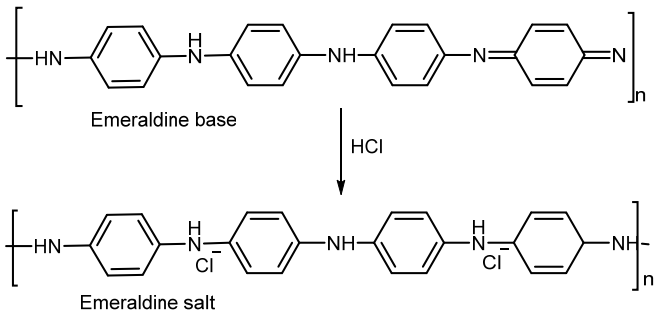

Fig 1. Chemical structure of PANI [13]

related to adsorbent and adsorbate (morphology of the adsorbent and functional group found in both and the porosity of adsorbent). As mentioned in the literature, adsorption capacity can be affected by the interaction of adsorbent and adsorbate, which depend on the pores present on the surface of the adsorbent. To solve this problem, many materials have been employed by mixing them with PANI, for example, carbon nanotubes [5], metal oxides and metals [6].

Through *in situ* chemical oxidation or electrochemical procedures, a number of different noble metal nanoparticle types, such as MnO_2 [7], Co_3O_4 [8], and MWCNTs/Fe_3O_4 [9], have recently been integrated into the PANI framework. Although there has been a lot of research on noble metal nanoparticles combined with conducting polymers, there is not a single study that sufficiently defines their use with increased reactivity, such as Nb_2O_5 and MnO_2, when combined with PANI nanofibers (i.e., PANI/Nb_2O_5/MnO_2 ternary nanocomposites). In this study, aniline monomer was used to polymerize with Nb_2O_5 and MnO_2 nanoparticles in an acidic aqueous media. Ammonium persulfate was used as the oxidant. This study's primary objective is to investigate the effects of pure PANI powder and a novel, highly porous adsorbent material termed as PANI/Nb_2O_5/MnO_2 ternary nanocomposite on the adsorption of MO dyes in the aqueous medium. The 4-dimethylaminoazobenzene-40-sulphonic acid sodium salt, also known as MO, is an anionic dye that is widely used in paper [10-11], pharmaceutical, textile and printing industries [12]. MO is highly soluble in water.

Several methods, including X-ray diffraction (XRD), Fourier transform infrared spectroscopy (FTIR) and scanning electron microscopy (SEM), were used to characterize the PANI/Nb_2O_5/MnO_2 ternary nanocomposite. The batch equilibrium and UV-vis spectroscopy methods were used to determine the high capacity of this sample in dye adsorption during the following tests: effects of pH solutions, start-up adsorbent dosage, contact time, and dye concentration. The adsorption process's kinetics, isotherms and thermodynamics have all been identified. The information offers hope for several important inferences, such as economic viability and a reusable adsorbent for color removal. Therefore, a unique method is being used to investigate the efficacy of a PANI/Nb_2O_5/MnO_2 ternary nanocomposite as an adsorbent for the removal of MO from wastewater.

■ EXPERIMENTAL SECTION

Materials

Water solutions are used in this study. The materials were utilized exactly as obtained from Sigma-Aldrich and included aniline monomer (99.5%), ammonium persulfate (APS, 98%), and acetone (99.5%). Without further purification, hydrochloric acid (Fisher Chemical, 37%), niobium(V) oxide (Fluka, 99%), chromium(III) oxide, ethanol, sodium hydroxide (99.8%), and manganese(IV) oxide (Panreac, 98%) were utilized.

Instrumentation

FTIR spectroscopy (PerkinElmer), X-ray diffractor (Model: Xrd-6000/Shimadzu, Japan), FE-SEM Thermo Fisher Scientific XL30, a UV-vis spectrophotometer (Shimadzu 1600, Japan), and pH meter (Oakton 550, USA) were used in this work.

Procedure

Synthesis of PANI/Nb_2O_5/MnO_2 adsorbent

Aniline (8 g) dissolved in 100 mL of 1 M HCl solution was then agitated for 1 h before being cooled for a further 30 min. Powder, 1 g of Nb_2O_5 and 1 g of MnO_2, was added straight to the solution by dissolving 14 g of the oxidant solution (APS) in an 80 mL aqueous solution of 1 M HCl; thus, the oxidant solution was synthesized.

So, by using the magnetic stirring method and a thermometer [14-15], aniline and metal oxide were combined. These were then slowly exposed to the APS solution, which was released dropwise from a separating funnel. To keep the temperature of the polymerization solution process at around 1–2 °C, 10 drops of APS were added per minute. The PANI nanocomposite had already been constructed when the polymerization reaction continued for 6 h and the arrangement's color slowly changed from grey to blue to green. The resulting PANI/Nb_2O_5/MnO_2 nanocomposite was washed with acetone, 1 L of 1 M HCl, newly distilled water and a Buchner funnel; lastly, the product was dried in a vacuum oven for 24 h at 70 °C [16]. Similarly, PANI/Nb_2O_5/Cr_2O_3 were synthesized in the same strategy that was used to prepare PANI/Nb_2O_5/MnO_2 described above (Fig. 2).

Batch adsorption experiments and experimental design

Due to their large surface area and superior adsorption capability, the as-synthesized PANI/Nb_2O_5/Cr_2O_3 and PANI/Nb_2O_5/MnO_2 nanocomposites are useful adsorbents for water and wastewater purification. This study identified MO since it is a typical organic contaminant in industrial sewage. A number of factors, including the pH of the solution, the amount of adsorbent used, the MO dye's starting concentration and the reaction time, were studied in relation to the removal of MO dye's adsorption to PANI/Nb_2O_5/Cr_2O_3 and PANI/Nb_2O_5/MnO_2 nanocomposites. A MO dye adsorption equilibrium experiment was carried out using two 250 mL conical flasks with a constant adsorbent dosage (100 mg) with initial concentrations of 100 mL of MO dye ranging from 10 to 200 mg/L. A pH meter was used to monitor the pH of the setups, which was adjusted to pH 7. To ensure equilibrium conditions, the orbital shakers were shaken at a controlled speed of 300 rpm after 60 min. By making use of a UV-vis spectrophotometer set to its maximum wavelength of 463 nm, a comparison of MO concentrations before and after was determined. Using

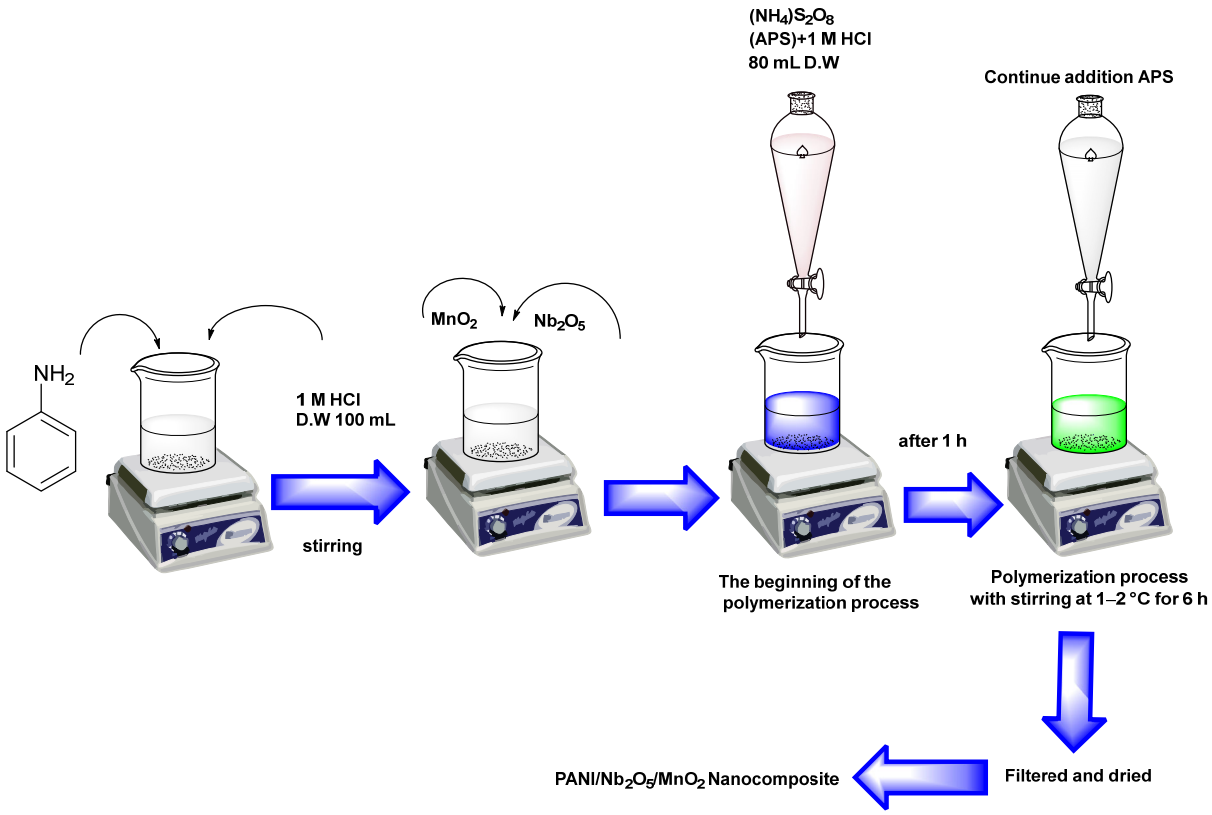

Fig 2. Schematic of the synthesis of PANI/Nb_2O_5/MnO_2 sample by *in situ* oxidative polymerization with its proposed interactions

the following methods, the percentage of dye removal (percent DR) was determined and noted in Eq. (1):

$$\text{Dye removal} = \frac{C_i - C_e}{C_i} \times 100 \quad (1)$$

where C_i is the initial concentration of MO dye (mg/L) and C_e is the equilibrium concentration of MO dye after adsorption (mg/L). The adsorption capacity (q_e) was calculated using Eq. (2):

$$q_e = \frac{(C_i - C_e)V}{M} \quad (2)$$

where: V is the volume of MO dye solution (L) and M is the weight of the adsorbent (g).

■ RESULTS AND DISCUSSION

Characterization of PANI/Nb_2O_5/Cr_2O_3 and PANI/Nb_2O_5/MnO_2

FTIR analysis

Fig. S1(a) and (b) display FTIR peaks for nanocomposites made of PANI/Nb_2O_5/Cr_2O_3 and PANI/Nb_2O_5/MnO_2 in the 400–4000 cm^{-1} range. It is clear from Fig. S1(a) and (b) that the peak at 3740 cm^{-1} is observed for all PANI samples, which results from the aromatic amines' N–H stretching [17]. The C–H stretch of the aromatic ring can be assigned to the range between 2933 and 3039 cm^{-1}. Although the peak at 1423 and 1464 cm^{-1} refers to the C=C stretching of the benzenoid rings; the peak at 1550 cm^{-1} is suggestive of the quinoid rings. At 1550 cm^{-1}, the C=N stretch reaches its maximum [16]. The C–H out-of-plane (o/p) bending vibration is maximized between 1097 and 1236 cm^{-1} [18]. The quinoid and benzenoid rings found in PANI/Nb_2O_5/MnO_2 suggested that the nanoparticles (Nb_2O_5, Cr_2O_3, and MnO_2) were functionalized with PANI, even though peak intensities were seen for PANI/Nb_2O_5/Cr_2O_3 and PANI/Nb_2O_5/MnO_2, and a set of broad bands was discovered between 489 and 792 cm^{-1}, confirming prior research findings that Nb–O, Cr–O and Mn–O interacted on the surface of PANI [19-20]. Tables 1 and 2 present the vibrational assignments for PANI/Nb_2O_5/MnO_2 and PANI/Nb_2O_5/Cr_2O_3 nanocomposites.

XRD analysis

Further attributes of the PANI/Nb_2O_5/Cr_2O_3 and PANI/Nb_2O_5/MnO_2 structures were researched with the means of XRD, as displayed in Fig. 3, to look at the crystallinity and undefined organization present in these

Table 1. FTIR peak assignments for PANI/Nb_2O_5/MnO_2

Assignment	Wavenumber (cm^{-1})
N–H stretching from aromatic amines group	3740
O–H stretching of hydroxyl group	3421
C–H stretching of aromatic unit	3039
C=C stretching of quinoid ring	1550
C=C stretching of benzenoid ring	1423
C–H bending	1236
N–H out-of-plan bending	794
Nb–O, Mn–O	563, 489

Table 2. FTIR peak assignments for PANI/Nb_2O_5/Cr_2O_3

Assignment	Wavenumber (cm^{-1})
N–H stretching from aromatic amines group	3740
O–H stretching of hydroxyl group	3493
C–H stretching of aromatic unit	2933
C=C stretching of quinoid ring	1550
C=C stretching of benzenoid ring	1464
C–H bending	1097
N–H out-of-plan bending	792
Nb–O, Cr–O	563,480

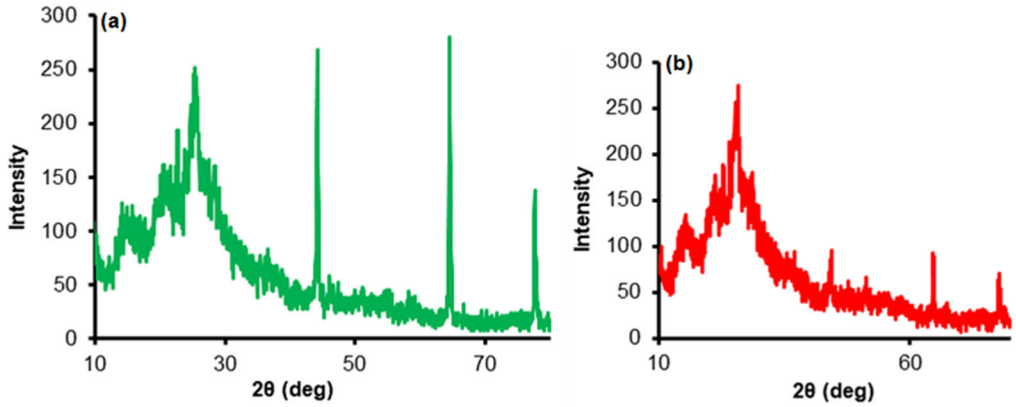

Fig 3. XRD spectra for (a) PANI/Nb_2O_5/MnO_2 and (b) PANI/Nb_2O_5/Cr_2O_3 samples

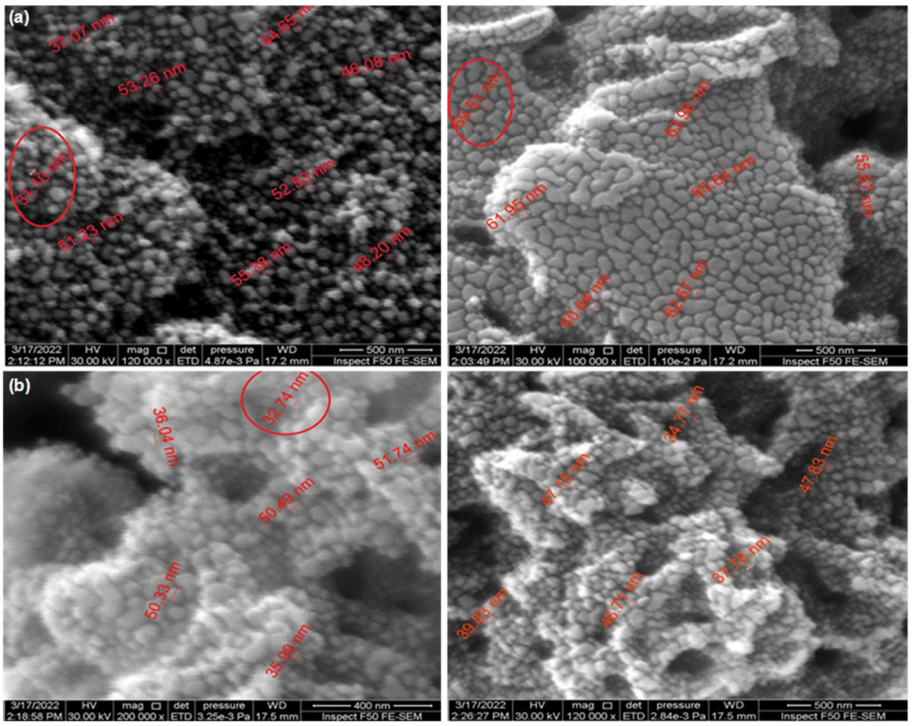

Fig 4. FE-SEM micrographs of (a) PANI/Nb_2O_5/MnO_2 and (b) PANI/Nb_2O_5/Cr_2O_3 nanocomposites

examples [21]. The wide peaks were seen at 2θ = 9.65°, 15.65°, 20.6°, 25.35°, 44.2°, 64.55° and 77.65°. These pinnacles confirmed that formless construction was available in PANI/Nb_2O_5/MnO_2 in the lattice [20,22]. While, the PANI/Nb_2O_5/Cr_2O_3 nanocomposite XRD tops were basically indistinguishable from the PANI precious stone planes with 2θ = 9.2°, 15.2°, 21.25° and 25.7°, 44.35°, 64.55° and 77.7° separately. The data showed that the metal oxides have adsorption interactions of a nanocrystalline type (Nb_2O_5 and additionally MnO_2, Cr_2O_3) and have a PANI network. This suggests that PANI was collaborating with Nb_2O_5, Cr_2O_3, and MnO_2 in the great precious stone construction. These outcomes (i.e., XRD) and the close FTIR results have demonstrated that the surface-based polymerization of the aniline monomer of the Nb_2O_5, Cr_2O_3, and MnO_2 nanoparticles [23-24] was successful.

Surface characterization by FE-SEM

The surface morphologies of artificial metal oxides/PANI nanocomposite were investigated via FE-SEM as shown in Fig. 4, where the morphology of Nb_2O_5, Cr_2O_3, and MnO_2 can be seen. The majority of

nanoparticles had spherical shapes and had sizes of around 30–68 nm. The PANI/Nb_2O_5/MnO_2 and the PANI/Nb_2O_5/Cr_2O_3 nanocomposites demonstrated that metal oxide nanoparticles had the same shape and were perfectly coated with thin polymer chains during the aggregation process [25-26]. It was assumed that there was a significant difference in morphology between the composites' surface and size of the PANI/Nb_2O_5/Cr_2O_3 and PANI/Nb_2O_5/MnO_2 nanocomposites. According to the XRD results, the chain diameter of the polymer nanocomposites ranged between 31 and 69 nm, changing the crystal growth's direction during adsorption. The doping of metal oxide nanoparticles in the polyaniline matrix was shown using FE-SEM.

Zeta potential analysis

The pH was 7.4, the zeta potential was 27.66 mV, and mobility was 2.16 V/cm. The addition of 20 mL of KCl resulted in a reduction in the zeta potential as well as an increase in particle size. At pH 10.2, around the isoelectric point, the biggest size was discovered. In other words, knowing the pH, adjusting and maintaining it at a stable value is required for PANI/Nb_2O_5/MnO_2 suspensions [27]. The electric potential created by a charge on a particle's surface, which can either have a positive or negative polarity depending on the particle's chemistry, is known as the zeta potential. The degree of repulsion between similarly charged particles in a formulation is measured by the zeta potential [28]. A formulation's zeta potential of PANI/Nb_2O_5/Cr_2O_3 indicates its likely physical stability from the changes in the zeta potential along with the particle size (Fig. 5). In the present study, the pH level was 7.4, the value of the zeta potential was 35.22 mV and mobility was 2.75 V/cm. Thus, it does seem to depend on

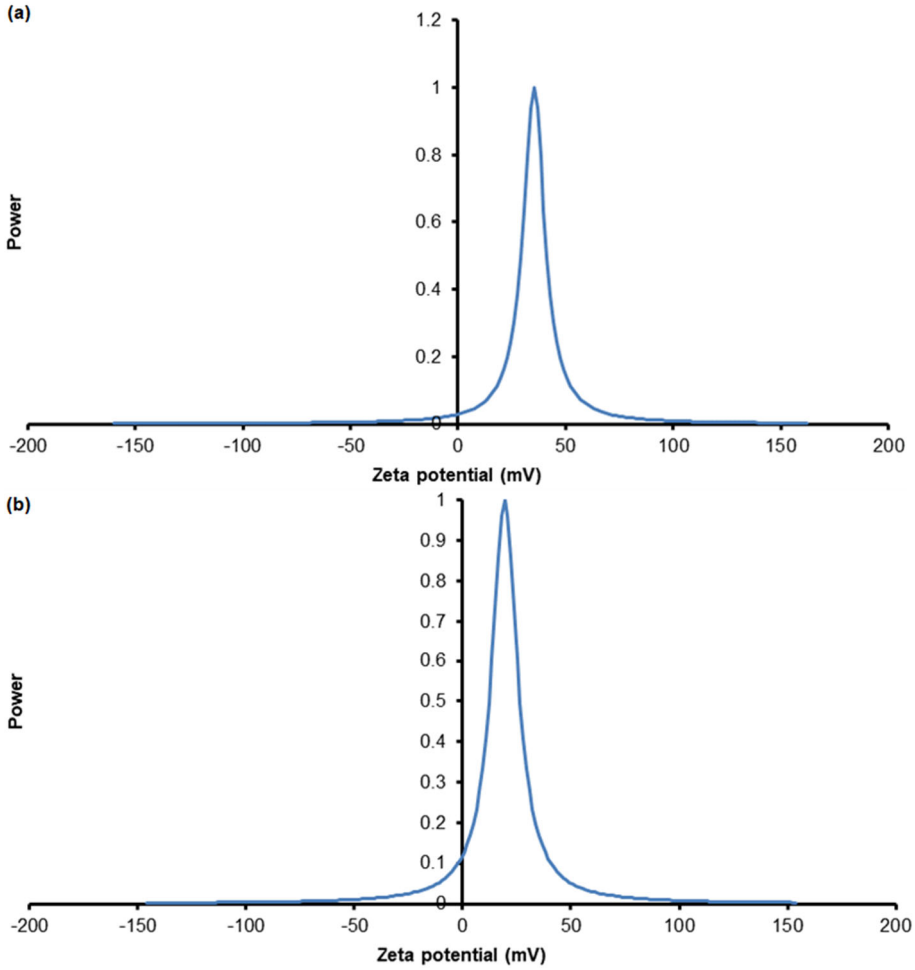

Fig 5. Zeta potential curves for (a) PANI/Nb_2O_5/MnO_2 and (b) PANI/Nb_2O_5/Cr_2O_3

the pH value. Moreover, the zeta potential increases with decreasing value of pH.

Optimization of as-synthesized PANI/Nb_2O_5/Cr_2O_3 and PANI/Nb_2O_5/MnO_2 nanocomposites as adsorbent for MO dye

Influence of adsorbent dosage

Removal tests were conducted using various concentrations of PANI/Nb_2O_5/Cr_2O_3 and PANI/Nb_2O_5/MnO_2, ranging from 10 to 150 mg, to discover the effects of adsorbent dose on MO dye clearance. The impact of the adsorbent dose on removal effectiveness for each dosage is shown in Fig. 6. The removal effectiveness of the MO dye was found to be greatly increased by increasing the adsorbent dosage from 10 to 50 mg for PANI/Nb_2O_5/Cr_2O_3, from 10 to 100 mg for PANI/Nb_2O_5/MnO_2, from 77.0–87.0% and 70.0–88.5%, respectively. This might be because more active sites became available when the adsorbent dosage was raised; eventually, at a dosage of 50 mg, the associated equilibrium was attained. For subsequent trials, an adsorbent dosage of 50 mg was chosen.

Influence of differences in initial concentration of MO dye on removal process

As shown in Fig. 7, the removal efficiency of PANI/Nb_2O_5/Cr_2O_3 and PANI/Nb_2O_5/MnO_2 was investigated using a variety of initial MO dye

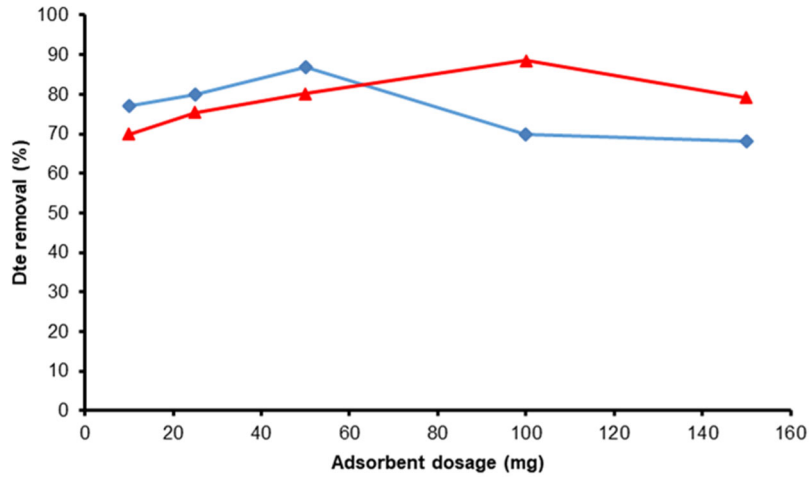

Fig 6. Effect of adsorbent dosage on the removal of MO dye using PANI/Nb_2O_5/MnO_2 (red) and PANI/Nb_2O_5/Cr_2O_3 (blue)

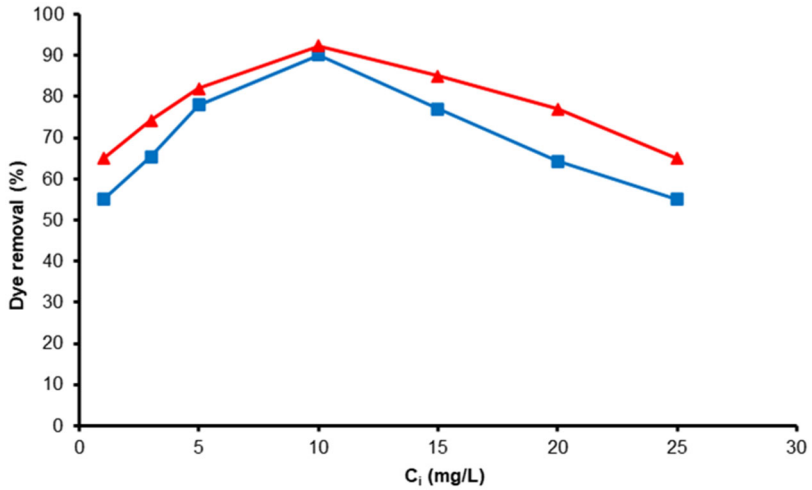

Fig 7. Effect of initial concentration of MO dye on the removal process using PANI/Nb_2O_5/MnO_2 (red) and PANI/Nb_2O_5/Cr_2O_3 (blue)

concentrations ranging from 1 to 25 mg/L at a fixed 50 mg of PANI/Nb_2O_5/Cr_2O_3 and 100 mg of PANI/Nb_2O_5/MnO_2. This graph shows that the original concentration of MO dye was increased. Accordingly, when the original MO dye concentration was increased, the removal effectiveness of the PANI/Nb_2O_5/Cr_2O_3 nanocomposite was high, demonstrating that each of the adsorbents and the MO dye molecules interacted strongly even at low starting concentrations [29]. Additionally, because of the larger surface area and strong electrostatic interactions, PANI/Nb_2O_5/Cr_2O_3 and PANI/Nb_2O_5/MnO_2 nanocomposites are two possible explanations for the effectiveness of these products in the removal of a high percentage of MO dye and the porosity of the adjusted PANI/Nb_2O_5/Cr_2O_3 and PANI/Nb_2O_5/MnO_2 being nanocomposite.

Influence of pH on removal of MO dye

Fig. 8 illustrates how pH affects the proportion of MO dye removed by nanocomposite materials made of PANI/Nb_2O_5/Cr_2O_3 and PANI/Nb_2O_5/MnO_2. Additionally, we investigated the initial and final (equilibrium) pHs. It is clear that at all chosen beginning pHs, the PANI/Nb_2O_5/MnO_2 nanocomposite outperformed PANI/Nb_2O_3/Cr_2O_3 in the removal of MO dye from the aqueous solution (from 2 to 10). To regulate the pH levels during the experiment, 0.1 M HCl or 0.1 M NaOH was used. The orbital shaking speed, quantity of both adsorbents and solution temperature were altered, while the starting MO dye concentration was held constant at 25 mg/L, 300 rpm, 50,100 mg, and 298 K. The findings of all the best studies pointed to the following: PANI/Nb_2O_5/Cr_2O_3 adsorbents performed better at pH 9 and PANI/Nb_2O_5/MnO_2 adsorbents at pH 7, respectively. Based on an estimated pKa value of MO, as a result, it becomes protonated at the initial pH values of 2 and 3 (pH is less than the pKa of MO), where it is primarily present in anionic form. Additionally, the presence of basic amine groups causes PANI to build a positive charge on its conductive backbone in an acidic media. Consequently, at initial acidic pH values, there was a significant degree of change in the removal rates of adsorbents. This was a result of electrostatic attraction between the positively charged PANI backbone and protonated MO dye molecules. Thus, PANI/Nb_2O_5/Cr_2O_3 nanocomposites for MO dye removal will decline [30-31]. The preferred initial pH range was 2 to 8, with neutral being the best value about 94.20% PANI/Nb_2O_5/Cr_2O_3 and 95.37% for another nanocomposite. This was because, at neutral pH, the MO would primarily take the anionic form, thereby increasing the number of electrostatic interactions between the MO dye and PANI/Nb_2O_5/Cr_2O_3 and PANI/Nb_2O_5/MnO_2 adsorbents [32].

Influence of adsorption time

Another important factor in the color removal process is the adsorption time. Through a series of adsorption experiments with adsorption time ranges between 10 and 120 min, the impact of adsorption duration on MO dye's adhesion to the PANI/Nb_2O_5/Cr_2O_3 and PANI/Nb_2O_5/MnO_2 adsorbents

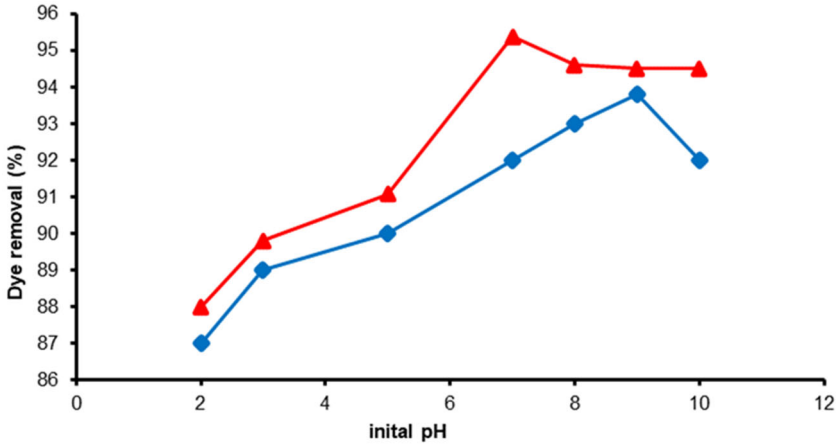

Fig 8. Effect of pH on removal of MO dye using PAI/Nb_2O_5/MnO_2 (red) and PANI/Nb_2O_5/Cr_2O_3 (blue)

was investigated. The results for each of the adsorbents are shown in Fig. 9. It is obvious that the removal rate of MO dye increases from 10 to 60 min and then stays constant from 60 to 120 min. Thus, upon following detour shaking for 60 min, equilibrium is attained in the MO dye adsorption. However, it should be noted that the rate of MO dye removal was extremely rapid during the first 10 min, during which time the MO dye molecules were adsorbent to around 94.2% of the PANI/Nb_2O_5/Cr_2O_3 and 97.8% of the PANI/Nb_2O_5/MnO_2 adsorbents before slowly and gradually increasing until equilibrium was reached at roughly 60 min. Since several active sites were available for MO dye molecules on both adsorbents' surfaces [32], the initial rapid removal of MO dye was explained. The number of active sites that could be removed decreased as the removal time rose; further, the pushing force decreased, resulting in a slow removal rate. As a result, the optimal adsorption time for subsequent research was chosen to be 60 min.

Batch MO Dye Adsorption Studies

Experimentally, it was found that the PANI/Nb_2O_5/Cr_2O_3 and PANI/Nb_2O_5/MnO_2 adsorbents' adsorption capabilities were best at pH 9 and 7, respectively, when used with 100 mL solutions of MO dye with concentrations ranging from 3 to 100 mg/L at room temperature (Fig. 10(a)). As can be seen from this figure, the maximal adsorption capabilities of the PANI/Nb_2O_5/Cr_2O_3 and PANI/Nb_2O_5/MnO_2 with similar amounts of adsorbents are 148 and 84 mg/g, respectively. Three fundamental isotherm models, specifically the Langmuir, Freundlich, and Temkin models, were used to fit the adsorption data in order to assess the mechanism of adsorption and provide information on the maximum adsorption capacity (q_m) for the relevant adsorbent [32]. The graphs of the isotherm parameters for the linearized equation for MO dye elimination at 298 K are shown in Fig. 10. The three equations for the isotherm models of adsorption at room temperature are listed in Table 3, together with their maximum adsorption capacities (q_m), correlation coefficients (R^2), and other data. Certain presumptions were connected with the Langmuir model, such as the monolayer adsorption of the adsorbate on an even surface of the adsorbent. In addition, chemisorption happens at designated homogenous sites inside the adsorbent to achieve adsorption. The Langmuir equation is given in Eq. (3) [33-34].

$$\frac{C_e}{q_e} = \frac{C_e}{q_m} + \frac{t}{q_m K_L} \quad (3)$$

where: q_m and q_e stand for the MO dye's maximum (mg/g) and empirical (q_e) adsorption capacities, respectively. After the adsorption process, C_e is the amount of MO dye that is still present in the solution, and K_L is the Langmuir constant (L/mg). In order to determine the adsorption capacity, C_e/q_e versus C_e was plotted (Fig. 10(b)).

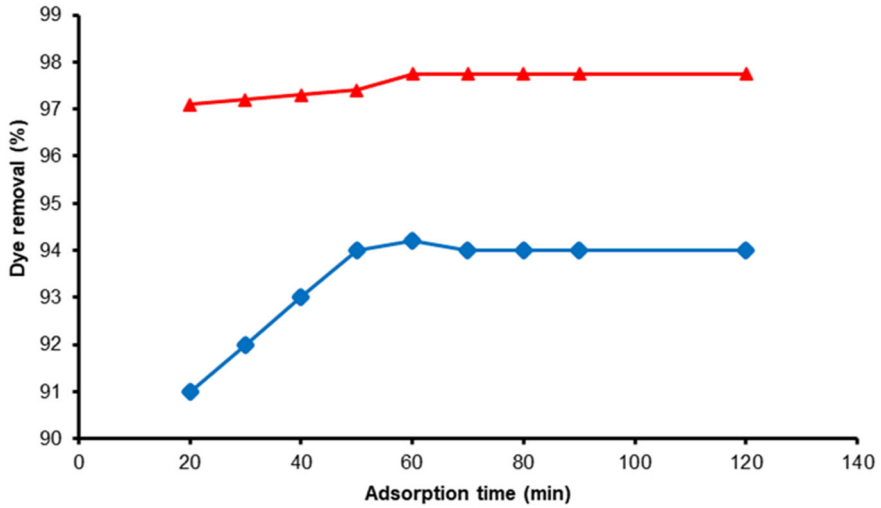

Fig 9. Effect of adsorption time on MO removal using PANI/Nb_2O_5/MnO_2 (red) and PANI/Nb_2O_5/Cr_2O_3 (blue)

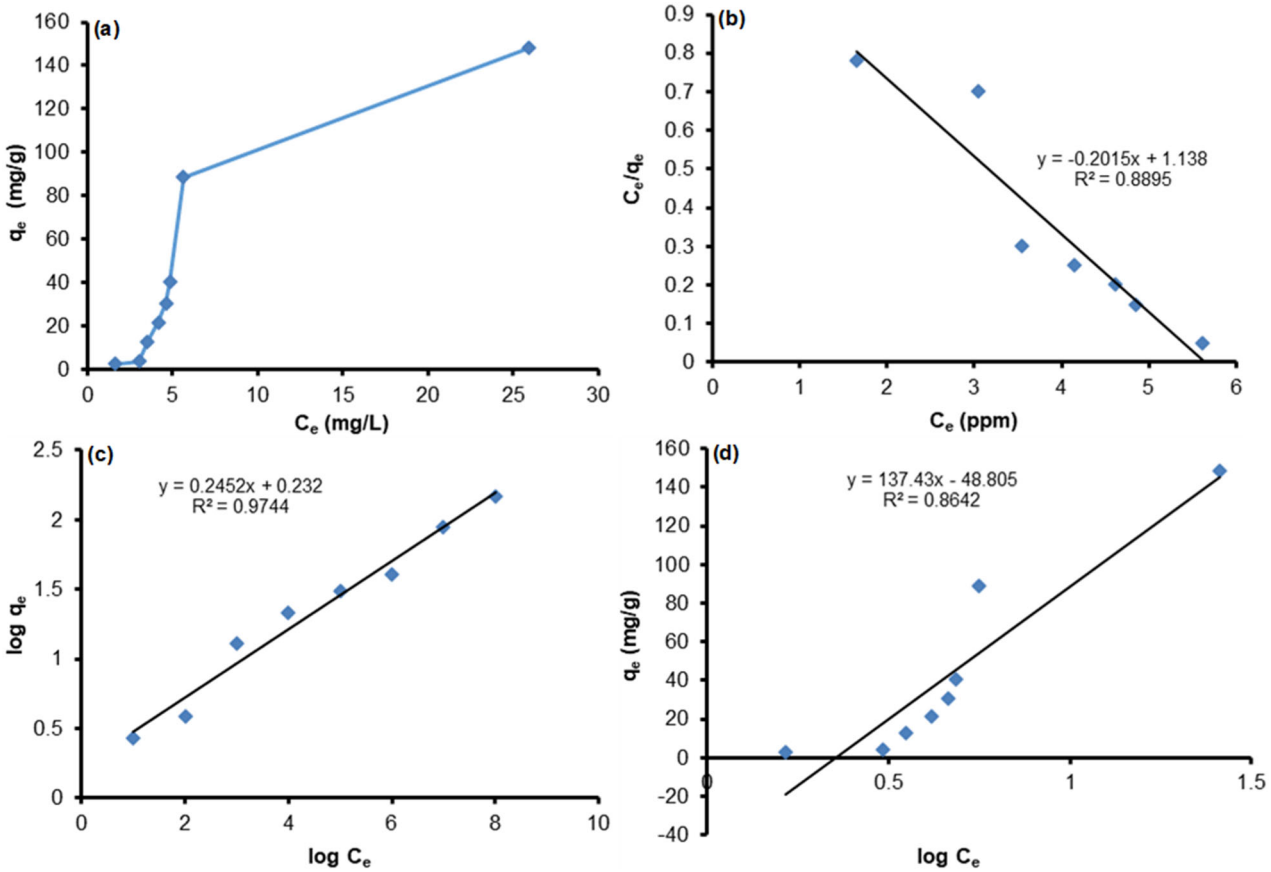

Fig 10. (a) Adsorption isotherms of MO onto PANI/Nb_2O_5/Cr_2O_3 adsorbents (conditions: pH 9; dosage = 50 mg; V = 100 mL; time = 60 min; T = 298 K). Fitting the adsorption isotherm curves of MO dye of adsorbents: (b) Langmuir, (c) Freundlich, and (d) Temkin isotherm models

Table 3. Adsorption Langmuir, Freundlich and Temkin model isotherm parameters for MO dye by PANI/Nb_2O_5/Cr_2O_3 and PANI/Nb_2O_5/MnO_2

Isotherms	Parameters	PNAI/Nb_2O_5/Cr_2O_3	PNAI/Nb_2O_5/MnO_2
	q_m (mg/g)	142	115
Langmuir	K_L (L/mg)	0.18	0.45
	R^2	0.8895	0.9150
	K_F (mg/g)(mg/L)$^{1/n}$	1.80	3.02
Freundlich	n	4.00	2.37
	R^2	0.9744	0.9398
	A	137.0	33.2
Temkin	B	48.00	2.38
	R^2	0.8640	0.9660

In Fig. 10 and 11, the gradient and intercept of this (straight) line were used to estimate q_m and K_L, respectively. The Freundlich model is used to fit multilayer adsorption onto a heterogeneous surface, and the postulated adsorption process is physisorption, which happens as a result of van der Waals interactions. Eq. (4) provides the Freundlich equation [35].

$$\log q_e = \log K_F + \frac{1}{n}\log C_e \quad (4)$$

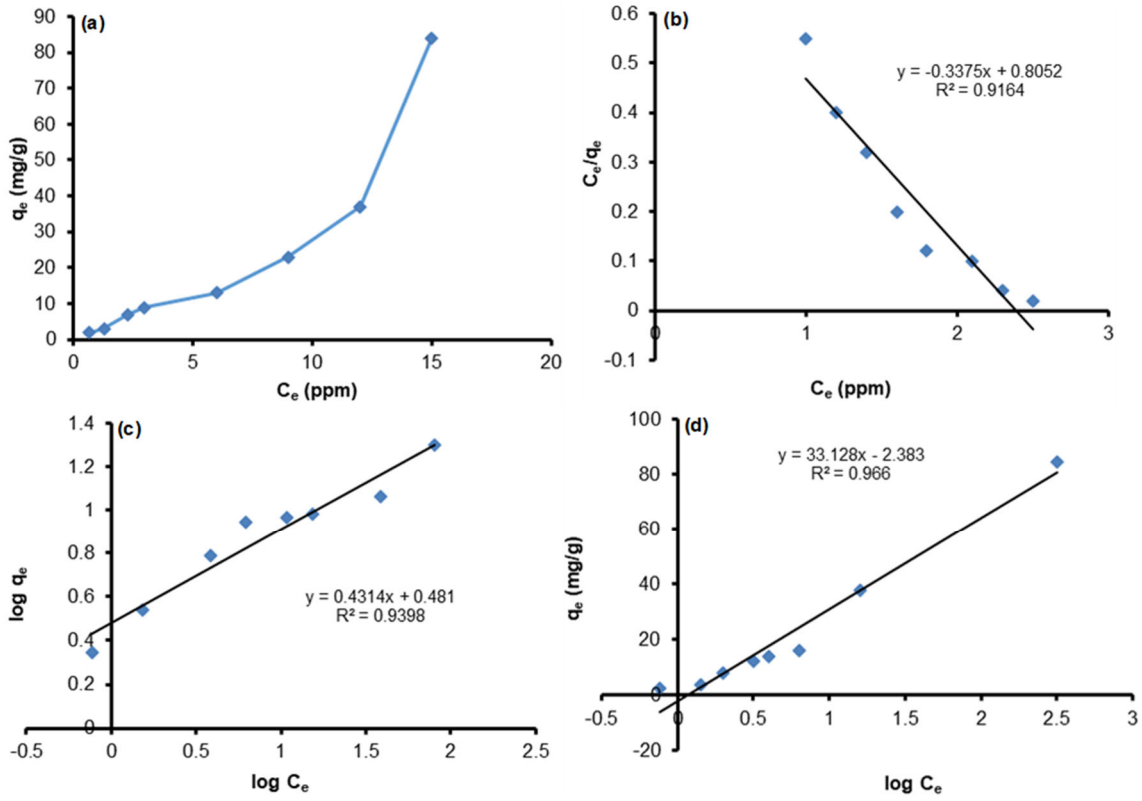

Fig 11. (a) Adsorption isotherms of MO onto PANI/Nb_2O_5/MnO_2 adsorbents (conditions: PH 7; dosage = 100 mg; V = 100 mL; time = 60 min; T = 298 K). Fitting the adsorption isotherm curves of MO dye of adsorbents: (b) Langmuir, (c) Freundlich, and (d) Temkin isotherm models

Table 4. Comparison of the removal efficiency of MO with different adsorbents

Adsorbent	q_m (mg g^{-1})	Adsorbent dose (g L^{-1})	Equilibrium time (min)	pH	References
PANI-MWCNT	149.25	0.040	60	7.0	[40]
PANI-AC	192.52	0.100	60	6.0	[41]
Co/Fe-MOF	137.60	0.005	60	4.0	[42]
PANI-TiO_2/GO	69.23	-------	80	-----	[43]
PANI/Nb_2O_5/MnO_2	76.00	0.100	60	7.0	This study
PANI/Nb_2O_5/Cr_2O_3	118.00	0.050	60	9.0	This study

According to Eq. (3), K_F stands for the Freundlich constant, while adsorption capacity (mg/g) and heterogeneity factor (n) stand for the bond distribution. By graphing log q_e against log C_e, the Freundlich linear equation was discovered. K_F and n were then accurately calculated from the intercept and slope, respectively, of this linear connection (Fig. 10(c)). Eq. (5) specifies the Temkin equation, where the Temkin isotherm model makes significant assumptions about heterogeneous surface energy and non-uniform distribution of sorption heat on adsorbents [36]

$$q_e = A + B \log C_e \quad (5)$$

where: A is the Temkin isotherm constant (L/g) and B is a constant related to the heat of adsorption (J/mol). Plots of q_e against log C_e were used to arrive at the Temkin linear equation (Fig. 10(d)). The gradient and intercept of the straight line provide the values of B and A, respectively. The parameters calculated for the

Langmuir, Freundlich, and Temkin models are listed in Table 3. The Langmuir isotherm appears to best describe the adsorption of MO dye against PANI/Nb_2O_5/Cr_2O_3 and PANI/Nb_2O_5/MnO_2 adsorbents, as evidenced by the coefficients of determination (R^2) for the fits of the experimental data of the three isotherms, which showed greater R^2 (0.9744 and 0.9398) and experimental equilibrium capacities (q_e). This implies that both the PANI/Nb_2O_5/Cr_2O_3 and PANI/Nb_2O_5/MnO_2 adsorbents have strong MO dye adsorption sites, and that the adsorption mechanism is monolayer in nature [37-39]. Table 4 represents the literature review of comparison of the removal efficiency of MO with different adsorbents.

■ CONCLUSION

In the current study, two types of the nanocomposite, PANI/Nb_2O_5/MnO_2 and PANI/Nb_2O_5/Cr_2O_3, were first prepared and characterized as new adsorbents to remove MO dye. The physical and chemical nature of the nanocomposites such as structural, morphological, particle size, and functional groups of the fabricated PANI/Nb_2O_5/MnO_2 and PANI/Nb_2O_5/Cr_2O_3 was established via XRD, FE-SEM, FTIR, UV-vis, and zeta potential, which can be summarized by showing that the adsorptive properties of nanocomposites were more active than pure PANI. The results have shown that the PANI/Nb_2O_5/Cr_2O_3 material has a higher adsorption capacity than PANI/Nb_2O_5/MnO_2 in terms of MO removal. The maximal adsorption capabilities reached 118 and 76 mg/g, respectively. The optimum conditions for the MO removal with PANI/Nb_2O_5/MnO_2 were the dose was 100 mg, the temperature was 298 K, and the pH value was 7. For PANI/Nb_2O_5/Cr_2O_3 nanocomposite, the dose was 50 mg, the temperature was 298 K, and the pH value was 9.

■ ACKNOWLEDGMENTS

The authors thank the University of Babylon for supporting this work.

■ AUTHOR CONTRIBUTIONS

Karrar Majeed Obaid did the laboratory work, Ahmed Saadoon Abbas wrote the experimental part, and Yahya Fahim Al-Khafaji wrote the rest of the paper.

■ REFERENCES

[1] Merdan, M., Jalal Al-den Fakar Al-den, D., Al-khafaji, Y., and Abbas, A.S., 2019, Theoretical study for chromen azodyes derivative compounds as anti-corrosive, *J. Phys.: Conf. Ser.*, 1234, 012054.

[2] Xiao, Y., and Hill, J.M., 2018, Benefit of hydrophilicity for adsorption of methyl orange and electro-Fenton regeneration of activated carbon-polytetrafluoroethylene electrodes, *Environ. Sci. Technol.*, 52 (20), 11760–11768.

[3] Sánchez-Sánchez, Á., Suárez-García, F., Martínez-Alonso, A., and Tascón, J.M.D., 2015, Synthesis, characterization and dye removal capacities of *N*-doped mesoporous carbons, *J. Colloid Interface Sci.*, 450, 91–100.

[4] Huang, R., Liu, Q., Huo, J., and Yang, B., 2017, Adsorption of methyl orange onto protonated cross-linked chitosan, *Arabian J. Chem.*, 10 (1), 24–32.

[5] Serban, G.V., Iancu, V.I., Dinu, C., Tenea, A., Vasilache, N., Cristea, I., Niculescu, M., Ionescu, I., and Chiriac, F.L., 2023, Removal efficiency and adsorption kinetics of methyl orange from wastewater by commercial activated carbon, *Sustainability*, 15 (17), 12939.

[6] Gapusan, R.B., and Balela, M.D.L., 2020, Adsorption of anionic methyl orange dye and lead(II) heavy metal ion by polyaniline-kapok fiber nanocomposite, *Mater. Chem. Phys.*, 243, 122682.

[7] Jianjun, H., Yuping, D., Jia, Z., Hui, J., Shunhua, L., and Weiping, L., 2011, γ-MnO_2/polyaniline composites: Preparation, characterization, and applications in microwave absorption, *Phys. B*, 406, 1950–1955.

[8] Shahabuddin, S., Sarih, N.M., Mohamad, S., and Atika Baharin, S.N., 2016, Synthesis and characterization of Co_3O_4 nanocube-doped polyaniline nanocomposites with enhanced methyl orange adsorption from aqueous solution, *RSC Adv.*, 6 (49), 43388–43400.

[9] Zhao, Y., Chen, H., Li, J., and Chen, C., 2015, Hierarchical MWCNTs/Fe_3O_4/PANI magnetic composite as adsorbent for methyl orange removal, *J. Colloid Interface Sci.*, 450, 189–195.

[10] Asuha, S., Zhou, X., and Zhao, S., 2010, Adsorption of methyl orange and Cr(VI) on mesoporous TiO_2 prepared by hydrothermal method, *J. Hazard. Mater.*, 181 (1), 204–210.

[11] Mohammadi, N., Khani, H., Gupta, V.K., Amereh, E., and Agarwal, S., 2011, Adsorption process of methyl orange dye onto mesoporous carbon material–kinetic and thermodynamic studies, *J. Colloid Interface Sci.*, 362 (2), 457–462.

[12] Zeng, A., and Zeng, A., 2017, Synthesis of a quaternized beta cyclodextrin-montmorillonite composite and its adsorption capacity for Cr(VI), methyl orange, and *p*-nitrophenol, *Water, Air, Soil Pollut.*, 228 (8), 278.

[13] Llorens, E., Armelin, E., Del Mar Pérez-Madrigal, M., Del Valle, L.J., Alemán, C., and Puiggalí, J., 2013, Nanomembranes and nanofibers from biodegradable conducting polymers, *Polymers*, 5 (3), 1115–1157.

[14] Alesary, H.F., Ismail, H.K., Khudhair, A.F., and Mohammed, M.Q., 2018, Effects of dopant ions on the properties of polyaniline conducting polymer, *Orient. J. Chem.*, 34 (5), 2525.

[15] Ismail, H.K., Alesary, H.F., Al-Murshedi, A.Y.M., and Kareem, J.H., 2019, Ion and solvent transfer of polyaniline films electrodeposited from deep eutectic solvents via EQCM, *J. Solid State Electrochem.*, 23 (11), 3107–3121.

[16] Bian, L.J., He, H.L., and Liu, X.X., 2015, Self-doped polyaniline/molybdenum oxide composite nanorods for supercapacitors, *RSC Adv.*, 5 (92), 75374–75379.

[17] Bakhtiarian, E., Foot, P.J., and Tate, P.C.M., 2016, Conductive poly(epichlorhydrin)–polyaniline dodecylbenzenesulfonate [PECH-PAni.DBSA] rubber blends prepared in solution, *Prog. Rubber Plast. Recycl. Technol.*, 32 (4), 183–200.

[18] Shahabuddin, S., Muhamad Sarih, N., Mohamad, S., and Joon Ching, J., 2016, $SrTiO_3$ nanocube-doped polyaniline nanocomposites with enhanced photocatalytic degradation of methylene blue under visible light, *Polymers*, 8 (2), 27.

[19] Cai, X., Cui, X., Zu, L., Zhang, Y., Gao, X., Lian, H., Liu, Y., and Wang, X., 2017, Ultra high electrical performance of nano nickel oxide and polyaniline composite materials, *Polymers*, 9 (7), 288.

[20] Wu, T.M., Lin, Y.W., and Liao, C.S., 2005, Preparation and characterization of polyaniline/multi-walled carbon nanotube composites, *Carbon*, 43 (4), 734–740.

[21] Inzelt, G., 2012, *Conducting Polymers: A New Era in Electrochemistry*, Springer Berlin, Heidelberg.

[22] Abd Ali, L., Ismail, H.K., Alesary, H.F., and Aboul-Enein, H., 2021, A nanocomposite based on polyaniline, nickel and manganese oxides for dye removal from aqueous solutions, *Int. J. Environ. Sci. Technol.*, 18 (7), 2031–2050.

[23] Mylarappa, M., Chandruvasan, S., Kantharaju, S., and Rekha, S., 2022, Synthesis and characterization of Rgo doped Nb_2O_5 nano composite for chemical sensor studies, *ECS Trans.*, 107, 269.

[24] Dessie, Y., Tadesse, S., and Eswaramoorthy, R., 2021, Surface roughness and electrochemical performance properties of biosynthesized α-MnO_2/NiO-based polyaniline ternary composites as efficient catalysts in microbial fuel cells, *J. Nanomater.*, 2021, 7475902.

[25] Taş, R., Can, M., and Sönmezoğlu, S., 2015, Preparation and characterization of polyaniline microrods synthesized by using dodecylbenzene sulfonic acid and periodic acid, *Turk. J. Chem.*, 39 (3), 589–599.

[26] Djara, R., Holade, Y., Merzouki, A., Masquelez, N., Cot, D., Rebière, B., Petit, E., Huguet, P., Canaff, C., Morisset, S., Napporn, T.W., Cornu, D., and Tingry, S., 2020, Insights from the physicochemical and electrochemical screening of the potentiality of the chemically synthesized polyaniline, *J. Electrochem. Soc.*, 167 (6), 066503.

[27] Fuseini, M., El Shazly, A.H., and El-Kady, M.F., 2020, Effects of doping on zeta potential and pH of polyaniline colloidal suspension, *Mater. Sci. Forum*, 1008, 114–120.

[28] Nawrocki, J., 1997, The silanol group and its role in liquid chromatography, *J. Chromatogr. A*, 779 (1), 29–71.

[29] Shahabuddin, S., Gaur, R., Mukherjee, N., Chandra, P., and Khanam, R., 2022, Conducting polymers-based nanocomposites: Innovative materials for waste water treatment and energy storage, *Mater. Today: Proc.*, 62, 6950–6955.

[30] Ansari, R., and Mosayebzadeh, Z., 2011, Application of polyaniline as an efficient and novel adsorbent for azo dyes removal from textile wastewaters, *Chem. Pap.,* 65 (1), 1–8.

[31] Nasar, A., and Mashkoor, F., 2019, Application of polyaniline-based adsorbents for dye removal from water and wastewater—A review, *Environ. Sci. Pollut. Res.*, 26 (6), 5333–5356.

[32] Harimu, L., Wahyuni, S., Nasrudin, N., Baari, M.J., and Permana, D., 2022, Fabrication of chitosan/Fe_3O_4 nanocomposite as adsorbent for reduction methylene blue contents, *Indones. J. Chem.*, 22 (3), 878–886.

[33] Karri, R.R., Tanzifi, M., Tavakkoli Yaraki, M., and Sahu, J., 2018, Optimization and modeling of methyl orange adsorption onto polyaniline nano-adsorbent through response surface methodology and differential evolution embedded neural network, *J. Environ. Manage.*, 223, 517–529.

[34] Al-Ghouti, M.A., and Da'ana, D.A., 2020, Guidelines for the use and interpretation of adsorption isotherm models: A review, *J. Hazard. Mater.*, 393, 122383.

[35] Ibrahim, R.K., El-Shafie, A., Hin, L.S., Mohd, N.S., Aljumaily, M.M., Ibraim, S., and AlSaadi, M.A., 2019, A clean approach for functionalized carbon nanotubes by deep eutectic solvents and their performance in the adsorption of methyl orange from aqueous solution, *J. Environ. Manage.*, 235, 521–534.

[36] Elwakeel, K., El-Bindary, A., Ismail, A., and Morshidy, A., 2017, Magnetic chitosan grafted with polymerized thiourea for remazol brilliant blue R recovery: Effects of uptake conditions *J. Dispersion Sci. Technol.*, 38 (7), 943–952.

[37] Manzar, M.S., Waheed, A., Qazi, I.W., Blaisi, N.I., and Ullah, N., 2019, Synthesis of a novel epibromohydrin modified crosslinked polyamine resin for highly efficient removal of methyl orange and eriochrome black T, *J. Taiwan Inst. Chem. Eng.*, 97, 424–432.

[38] Elwakeel, K.Z., El-Bindary, A., El-Sonbati, A., and Hawas, A.R., 2017, Magnetic alginate beads with high basic dye removal potential and excellent regeneration ability, *Can. J. Chem.*, 95 (8), 807–815.

[39] Sharifpour, E., Alipanahpour Dil, E., Asfaram, A., Ghaedi, M., and Goudarzi, A., 2019, Optimizing adsorptive removal of malachite green and methyl orange dyes from simulated wastewater by Mn-doped CuO-nanoparticles loaded on activated carbon using CCD-RSM: Mechanism, regeneration, isotherm, kinetic, and thermodynamic studies, *Appl. Organomet. Chem.*, 33 (3), e4768.

[40] Pete, S., Kattil, R.A., and Thomas, L., 2021, Polyaniline-multiwalled carbon nanotubes (PANI-MWCNTs) composite revisited: An efficient and reusable material for methyl orange dye removal, *Diamond Relat. Mater.*, 117, 108455.

[41] Bekhoukh, A., Moulefera, I., Zeggai, F.Z., Benyoucef, A., and Bachari, K., 2022, Anionic methyl orange removal from aqueous solutions by activated carbon reinforced conducting polyaniline as adsorbent: Synthesis, characterization, adsorption behavior, regeneration and kinetics study, *J. Polym. Environ.*, 30 (3), 886–895.

[42] Tran, K.N.T., Phan, C.P.K., Ho, V.T., Chau, H.D., and Nguyen, T.N.D., 2023, Adsorption of methyl orange dyes on oriented Co/Fe-MOF bimetallic organic framework in wastewater treatment, *Indones. J. Chem.*, 23 (2), 533–541.

[43] Mohammadi, R., Massoumi, B., and Galandar, F., 2019, Polyaniline-TiO_2/graphene nanocomposite: An efficient catalyst for the removal of anionic dyes, *Desalin. Water Treat.*, 142, 321–330.